Received: 21 January 2019 | Revised: 15 May 2019 | Accepted: 19 June 2019

DOI: 10.1002/jez.2308

JEZ-A ECOLOGICAL AND INTEGRATIVE PHYSIOLOGY WILEY

RESEARCH PAPER

Malaria mosquitoes use leg push-off forces to control body pitch during take-off

Wouter G. van Veen | Johan L. van Leeuwen | Florian T. Muijres

Experimental Zoology Group, Department of Animal Sciences, Wageningen University, Wageningen, The Netherlands

Correspondence
Florian T. Muijres, Experimental Zoology Group, Wageningen University, P.O. Box 338 6700AH Wageningen, The Netherlands.
Email: Florian.Muijres@wur.nl

Funding information
The Netherlands Organization for Scientific Research, Grant/Award Number: NWO/VENI-863-14-007

Abstract

Escaping from a blood host with freshly acquired nutrition for her eggs is one of the most critical actions in the life of a female malaria mosquito. During this take-off, she has to carry a large payload, up to three times her body weight, while avoiding tactile detection by the host. What separates the malaria mosquito from most other insects is that the mosquito pushes off gently with its legs while producing aerodynamic forces with its wings. Apart from generating the required forces, the malaria mosquito has to produce the correct torques to pitch-up during take-off. Furthermore, the fed mosquito has to alter the direction of its aerodynamic force vector to compensate for the higher body pitch angle due to its heavier abdomen. Whether the mosquito generates these torques and redirection of the forces with its wings or legs remains unknown. By combining rigid-body inverse dynamics analyses with computational fluid dynamics simulations, we show that mosquitoes use leg push-off to control pitch torques and that the adaption of the aerodynamic force direction is synchronized with modulations in force magnitude. These results suggest that during the push-off phase of a take-off, mosquitoes use their flight apparatus primarily as a motor system and they use leg push-off forces for control.

KEYWORDS
aerodynamics, *Anopheles coluzzii*, computational fluid dynamics

1 | INTRODUCTION

Females of most mosquito species depend on a blood-meal to acquire the needed nutrition for reproduction (Clements, 2011), however obtaining this blood meal is not without risk (Roitberg, Mondor, & Tyerman, 2003). The gravid mosquito has to find and land on a host, consume the blood, and take-off all without being detected. The host-seeking behavior and blood feeding have been studied in detail (Clements, 2011; Takken, 1991), but less is known about the take-off (Roitberg et al., 2003).

To increase its chance to successfully fly away, a mosquito needs to maximize its escape velocity within the constraint of avoiding tactile detection by the host (Muijres et al., 2017). Maintaining a high escape velocity becomes particularly challenging for blood-fed mosquitoes, because a mosquito can triple in weight due to a blood-meal (Clements, 2011; Roitberg et al., 2003), which in combination with the absence of large forces generated by the legs, puts even more strain on the flight apparatus. The escape velocity scales inversely with the size of the blood-meal and consequently with the survival chance (Roitberg et al., 2003).

During the take-off of an insect, the flight apparatus can either be started before take-off, during take-off or after take-off (Chen & Sun, 2014). Insects adopting the first take-off strategy, such as the butterfly (Sunada, Wtanabe, & Azuma, 1993) and the drone-fly (Chen & Sun, 2014), rely almost completely on the generation of aerodynamic forces with their wings. Insects adopting the last

take-off mechanics rely on the forces generated by the legs to generate the upward acceleration, for instance, found in the escape response of the fruit fly (Card & Dickinson, 2008) and the take-off of the locust (Pond, 1972). Finally, many insects combine leg forces with aerodynamic forces to generate the upward acceleration, for example, the voluntary take-off of the fruit fly (Chen & Sun, 2014; Card & Dickinson, 2008). It has been suggested that mosquitoes avoid tactile detection by extending their legs while generating aerodynamic forces with their wings (Muijres et al., 2017; Smith, Clayton, Khan, & Dickerson, 2018), keeping the force on the substrate lower than the tactile detection threshold of mammalian skin ($F_{threshold}$ = 0.07 mN; Li et al., 2011). This may explain why the difference between a voluntary take-off and escape take-off in the fruit fly is not found in mosquitoes (Muijres et al., 2017).

How the aerodynamic forces and torques required for take-off are generated by the mosquito remains unknown (Muijres et al., 2017). One of the possible explanations of the remarkable lifting capabilities of the mosquitoes may be caused by the interaction of wingbeat-induced air movement with the substrate from where the animal flies away, known as the ground effect. Although no ground effect has been found in similarly sized insects, such as the fruit fly (Kolomenskiy et al., 2016), the mosquito does not jump in the air but starts flapping its wings close to the ground. The closer proximity of the flapping mosquito wing to the substrate may lead to ground reaction forces to aid in the mosquito's take-off.

Another explanation is the increase of the stroke amplitude during take-off, which is linked to an increase in force production (Muijres et al., 2017). Other insects that are able to carry large payloads employ a similar wingbeat kinematics as the mosquito (Altshuler, Dickson, Vance, Roberts, & Dickinson, 2005; Bomphrey, Nakata, Phillips, & Walker, 2017); using a shallow stroke amplitude during steady-hovering flight, enables the insect to increase its stroke amplitude when accelerating the body or carrying large payloads.

Apart from generating enough forces, the mosquito has to correct its body pitch angle, which is nose-down at the start of the take-off, to a nose-up orientation to ensure a more horizontal stroke-plane of the wingbeat (Muijres et al., 2017). The required pitch-up torque can be generated by the legs, as seen in the take-off of fruit flies (Chen & Sun, 2014), or by adapting the wing kinematics as applied by maneuvering fruit flies in free flight (Muijres, Elzinga, Melis, & Dickinson, 2014; Dickinson & Muijres, 2016; Karasek, Muijres, De Wager, Remes, & Croon, 2018). It remains an open question how the mosquito controls its body pitch during the take-off.

In this study, we focused on the forces and torques generation during take-off of the malaria mosquito (*Anopheles coluzzii*; Muijres et al., 2017), clarified by combining rigid-body inverse dynamics analyses with state of the art computational fluid dynamics (Bhalla, Bale, Griffith, & Patankar, 2013). Our analysis suggests that the ground effect plays no role in aerodynamic force production during take-off of the mosquito, despite the close proximity of the beating wings to the ground. Furthermore, the aerodynamic force vector aligns closer to the body with increasing total force to compensate for the pitch-up orientation due to the heavy abdomen of a blood-fed female mosquito. Last, the pitch-up body movement throughout the take-off is primarily controlled by modulating the leg push-off forces exerted on the ground, which in turn, change the pitch torques.

2 | MATERIALS & METHODS

2.1 | Experimental animals and conditions

Here, we combined rigid-body inverse dynamics analyses with computational fluid dynamics (CFD) to study the take-off dynamics of 13 female malaria mosquitoes (*Anopheles coluzzii*). Six take-off maneuvers were of non-blood-fed mosquitoes, and seven of blood-fed malaria mosquitoes; the kinematics of these maneuvers were previously published (Muijres et al., 2017). The inverse dynamics method provided us with total force and torque dynamics throughout each maneuver and the CFD simulations allowed us to determine the aerodynamic forces and torques produced by the flapping wings. By subtracting aerodynamic forces and torques from the total forces and torques, we estimated the contribution of the leg push-off to force and torque production.

For one take-off of a lean mosquito and one of a blood-fed mosquito, we performed CFD simulations both with and without a take-off platform to evaluate the effect of the presence of the ground on the aerodynamic forces and torques acting on the mosquitoes.

2.2 | Computational fluid dynamics solver

We used CFD based on the immersed boundary methods (Bhalla et al., 2013) to simulate the forces, torques, and the flow-field as a result of the wing and body motion of the mosquito during take-off. The immersed boundary method enabled us to simulate the complex movement of the mosquito, without having to take complex mesh deformations of traditional CFD methods into account (Mittal & Iaccarino, 2005).

The simulations were conducted on a domain of size 140 mm on all sides (Figure 1a,b and Movies S1,S2). The domain size was chosen such that negligible interaction between the airflow generated by the mosquito and the domain boundaries occurred, except for the bottom boundary, because we simulated a mosquito taking off from the ground. On all boundaries, a no-slip boundary is enforced, such that all boundaries act as an impenetrable wall. On the body of the mosquito, a no-slip boundary condition was enforced using the forcing function of the immersed boundary method (Bhalla et al., 2013).

Both the motion and the shape of the mosquito were prescribed during the simulation. The motion of the body and wings arises from the measured kinematics, the shape of the mosquito comes from the combined shape of the body and wings (Figure 1c,d). Wing geometry scales isometrically with wing length and all wings had a thickness of 0.03 mm (~1% of the wing length). All mosquitoes had a body length

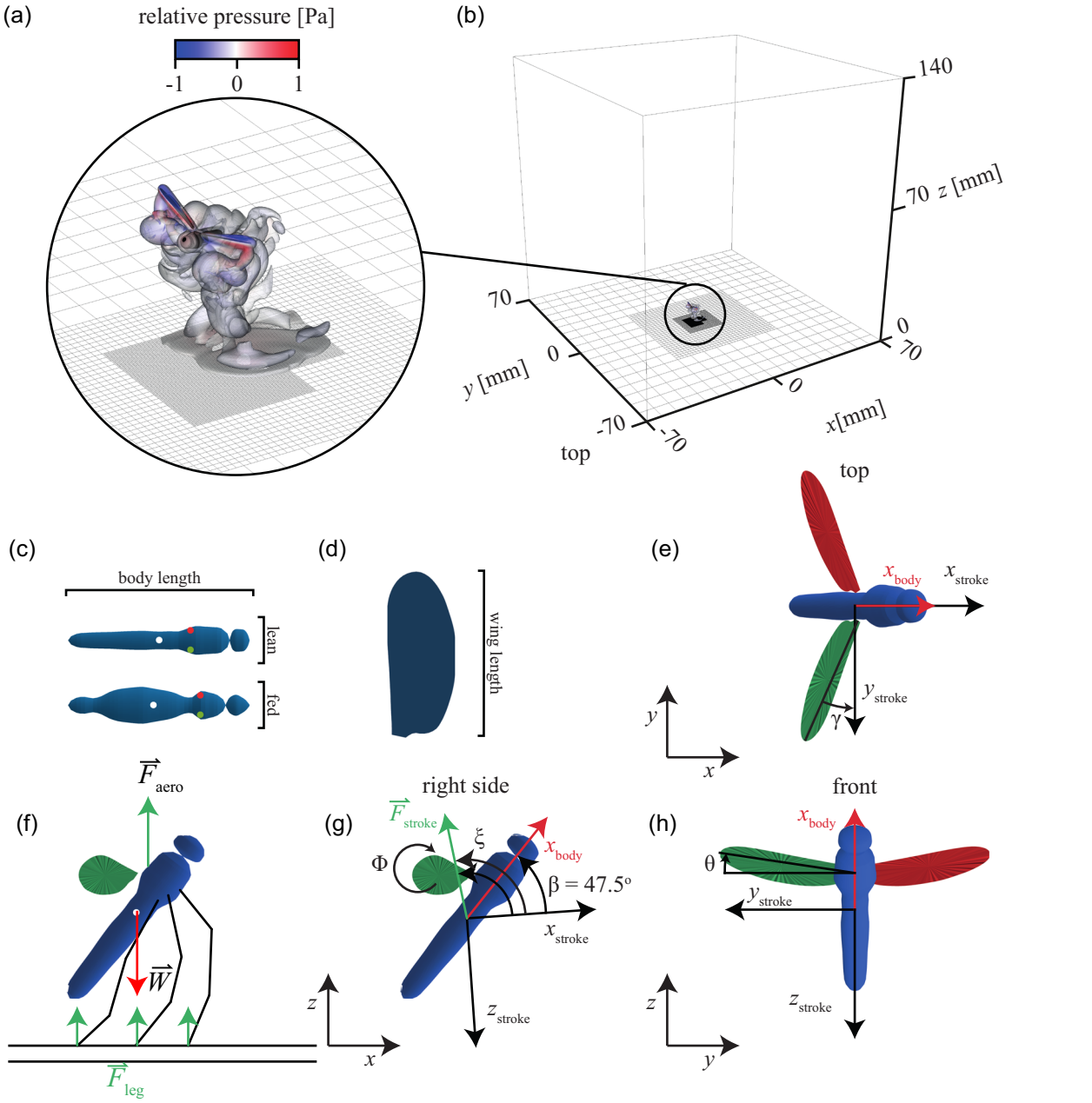

FIGURE 1 (a) Wake structure visualization using an isosurface with a vorticity threshold of 1,000 s^{-1}, colored by relative pressure. (b) Domain setup: within the circle the solution of a take-off is shown (see (a)). (c, d) Body and wing geometries used for the simulations, wings are isometrically scaled with length, white dot is the center of mass, green and red dot are the right and left wing roots, respectively. (e, g, h) A mosquito with the right wing in green and left wing in red, viewed from the top (e), side (g) and front (h), including wing kinematics parameters and definition of the stroke-plane reference frame and world-reference frame. The wingbeat kinematics parameters are stroke angle γ (e), stroke-plane angle β, force angle ξ, the wing pitch angle ϕ (g), and the deviation angle θ (h). (f) Free body diagram of a mosquito taking off from a substrate, with the weight vector $\vec{W}$ in red, and in green the forces produced by the mosquito. These consist of the aerodynamic force produced by the beating wings $\vec{F}_{aero}$, and the ground reaction forces resulting from leg push-off $\vec{F}_{leg}$ [Color figure can be viewed at wileyonlinelibrary.com]

of 4.7 mm, and the shape of the body was kept constant for all lean mosquitoes and blood-fed mosquitoes; for the computation of the center of mass, it is assumed that the mass is homogeneously distributed in the mosquito.

To accurately compute the complex fluid dynamics close to the mosquito, we used an adaptive mesh refinement (AMR) algorithm that refines the mesh based on areas in the flow-field with high-vorticity. This resulted effectively in a refinement close to the body and in the wake. At the finest refinement level, a refinement of $\Delta x = 0.0304$ mm was used, which led to a mesh size of approximately 4 million cells. After the choice of the refinement level, a corresponding time-step was chosen of $\Delta t = 1 \times 10^{-7}$ s. We validated the solver in a previous study (van Veen, van Leeuwen, & Muijres, 2019), using the wingbeat kinematics of a hovering fruit fly and the

corresponding aerodynamic forces, determined using a robotic flapper experiment (Muijres et al., 2014). The forces simulated by our method are similar to the forces predicted in the robotic experiment (see Supporting Information Methods for more detail).

2.3 | Reference frames

In this study, two reference frames were used; the world-reference frame, and the stroke-plane reference frame. The world-reference frame is a right-handed orthogonal reference frame with its origin at the center of the domain at ground level (Figure 1b). To simulate a take-off without a ground present, the start of the take-off was placed 70 mm above the bottom of the simulation domain.

The stroke-plane reference frame is a right-handed orthogonal reference frame attached to the center of mass of the body of the mosquito (Figure 1e,g,h) and aligned with the stroke-plane of an average wingbeat. Its *y*-axis is pointing to the right side of the animal, the *x*-axis pointing forward in the direction of the head, and pitched down relative to the body axis with a constant stroke-plane angle $\beta = 47.5°$ (Figure 1g); the *z*-axis pointing down towards the ventral side of the mosquito (Figure 1e,g,h).

2.4 | Kinematics

The body and wing motion of the mosquito take-offs were obtained from a previous study (Muijres et al., 2017). The rotation and location of the body were prescribed in the world-reference frame (Figure 1b). The motion of the wings was described in the stroke-plane reference frame (Figure 1e), using three Euler angles; the stroke angle, the deviation angle and the wing rotation angle. First, the stroke angle (γ, Figure 1e) describes the forward and backward motion within the stroke-plane of the wing, where for a zero-stroke angle the wing is aligned with the *y*-axis. Second, the deviation angle (θ, Figure 1h) describes the wing angle out of the stroke-plane, where for positive deviation angles the wing is pointing towards the dorsal side of the body. Finally, the wing rotation angle (ϕ, Figure 1g) describes the rotation of the wing around its longitudinal axis, where a zero angle defines a vertical wing with the leading edge pointing upwards.

2.5 | Force analysis

Throughout a take-off, the total force produced by a mosquito, $\vec{F}_{\text{total}}$, consist of the aerodynamic force, $\vec{F}_{\text{aero}}$, and the ground reaction forces on the legs, $\vec{F}_{\text{leg}}$. The total forces were computed in the world-reference frame from the kinematics using inverse rigid-body dynamics as

$$(\vec{F}_{\text{total}})_{\text{world}} = m_{\text{mosq}} \frac{d}{dt}(\vec{V}_{\text{world}}) - \vec{W}, \tag{1}$$

where m_{mosq} is the mass of the mosquito, $\vec{V}_{\text{world}}$ the velocity vector of the body in the world-reference frame, and $\vec{W}$ the weight of the mosquito ($\vec{W} = [0; 0; -m_{\text{mosq}}g]$, where $g = 9.81\ \text{m s}^{-2}$).

The aerodynamic forces computed by the CFD solver were also determined in the world reference frame. These aerodynamic forces fluctuate highly throughout each wingbeat, and therefore we estimated the wingbeat-average aerodynamic forces, $\vec{F}_{\text{aero}}$, using a fifth-order Butterworth filter ($f_{\text{low}} = 1\times 10^{-6}$ Hz and $f_{\text{high}} = 200$ Hz). The leg-derived forces were estimated as the difference between the total aerodynamic forces and the wingbeat-average aerodynamic forces as $\vec{F}_{\text{leg}} = \vec{F}_{\text{total}} - \vec{F}_{\text{aero}}$.

To compute the angle between the aerodynamic force vector and the stroke-plane, the forces derived from the CFD solver $\vec{F}_{\text{aero}}$ were first transformed to the stroke-plane reference frame by

$$(\vec{F}_{\text{aero}})_{\text{stroke}} = \mathbf{A}^T_{\text{stroke}} \mathbf{A}^T_{\text{body}} (\vec{F}_{\text{aero}})_{\text{world}}, \tag{2}$$

where $\mathbf{A}_{\text{stroke}}$ is the rotation matrix from the body-reference frame to the stroke-plane reference frame and $\mathbf{A}_{\text{body}}$ the rotation matrix that describes the motion of the body in the world-reference frame.

From the forces in the stroke-reference frame, the angle between the force and the stroke-plane (Figure 1f) was computed as

$$\xi = \tan^{-1}\left(\frac{(F_z)_{\text{stroke}}}{\text{sign}(F_x)_{\text{stroke}} \sqrt{(F_x)^2_{\text{stroke}} + (F_y)^2_{\text{stroke}}}} \right). \tag{3}$$

All forces were either normalized with the weight of the animal as $\vec{F}^* = \vec{F}/(m_{\text{mosq}}g)$, or with a generic weight $\vec{F}^{**} = \vec{F}/(m_{\text{gen}}g)$, with $m_{\text{gen}} = 1$ mg.

2.6 | Torque analysis

Similar to the forces, the torques produced by the mosquito were also expressed in the stroke-plane reference frame, using the reference frame transformation described in equation (2). The resulting stroke-plane-based torques consist of roll torque about the *x*-axis, pitch torque about the *y*-axis, and yaw torque about the *z*-axis.

The total torques produced by the mosquito were computed based on the kinematics using rigid-body inverse dynamics in two steps: first, we computed the angular momentum of the mosquito in the stroke-plane reference frame as

$$(\vec{\mathcal{L}}_{\text{total}})_{\text{stroke}} = \mathbf{I}\vec{\omega}_{\text{stroke}}, \tag{4}$$

where $\mathbf{I}$ is the moment of inertia matrix of the mosquito, and $\vec{\omega}_{\text{stroke}}$ the angular velocity of the mosquito in the stroke-plane reference frame. Second, the total torque produced by the mosquito was computed as

$$(\vec{T}_{\text{total}})_{\text{stroke}} = \frac{d}{dt}(\vec{\mathcal{L}}_{\text{total}})_{\text{stroke}}. \tag{5}$$

The equivalent aerodynamic torques produced by the beating wings were estimated using CFD. Like the forces, these torques vary highly throughout each wingbeat, and therefore we estimated the wingbeat-average aerodynamic torques, $\vec{T}_{\text{aero}}$, using a fifth-order Butterworth filter ($f_{\text{low}} = 1 \times 10^{-6}$ Hz and $f_{\text{high}} = 200$ Hz; Jones,

Oliphant, & Peterson, 2001). The angular momentum that would result from aerodynamic torque production alone, was estimated by numerically integrating the aerodynamic torques throughout each take-off maneuver.

The corresponding torques and angular momentum produced by leg push-off were consequently estimated as $\vec{T}_{leg} = \vec{T}_{total} - \vec{T}_{aero}$ and $\vec{\mathcal{L}}_{leg} = \vec{\mathcal{L}}_{total} - \vec{\mathcal{L}}_{aero}$, respectively. All torques were then normalized with the product of body weight and body length of the animal, $\vec{T}^* = \vec{T}/(m_{mosq} g l_{mosq})$.

Throughout a take-off, a mosquito primarily pitches up, and thus we primarily focused on pitch torque production. To study the effect of the different pitch torque components on this pitch dynamics, we defined the contribution of pitch torque on pitch angle change ε_{pitch}. This parameter can be calculated by integrating the angular momentum throughout the push-off phase of the take-off as

$$\varepsilon_{pitch} = I^{-1} \sum_{i=0}^{n_{lift-off}} (\vec{\mathcal{L}}_i)_{pitch}, \quad (6)$$

whereby I^{-1} is the inverse of the moment of inertia, $n_{lift\text{-}off}$ is the time-step at which the last leg leaves the ground, and $\vec{\mathcal{L}}_i$ either the total, aerodynamic or leg contribution to the angular momentum at time-step i.

3 | RESULTS

We performed rigid-body inverse dynamics analyses and CFD simulations of the take-off maneuvers of six lean mosquitoes and seven blood-fed mosquitoes. Typical examples of the simulations for a lean and fed mosquito are shown in Movie S1 and Movie S2, respectively.

3.1 | Ground effect

The two cases highlighted in Movies S1 and S2 were also used to study the ground effect. For this, we repeated these simulations, with the only difference being the absence of the grounds. A patch of the ground surface (2 cm × 2 cm) was extracted when the air pressure acting on the ground was maximum (Figure 2a–d). The maximum air pressure planes with the ground present (Figure 2a,c) show larger pressure fluctuations when compared with the planes without a ground present (Figure 2b,d). The air pressure acting on the ground surface of 2 cm × 2 cm was extracted for all the time-steps during the push-off phase and integrated over the surface. The resulting forces fluctuate during the take-off, but for all simulated lean mosquitoes the average maximum force ($F_{substrate}$ = 0.05 ± 0.01 mN; n = 6) remain below the force detection threshold of mammalian skin ($F_{threshold}$ = 0.07 mN; Figure 2i; Li et al., 2011). The average maximum forces for the blood-fed mosquitoes is equal to the detection threshold ($F_{substrate}$ = 0.07 ± 0.01 mN; n = 7). The averaged pressure forces are considerably lower than the forces generated by the legs, and only alter the total averaged forces acting on the substrate slightly (Figure 2i,j).

Interestingly, the large differences in ground pressure between the simulations with and without ground do not lead to large differences in the wake structure (Figure 2e–h). For the case with the ground present, the wake is interacting with the ground but no large change is propagated further towards the insect (Figure 2e,g). Furthermore, no difference can be observed in the aerodynamic forces on the body and wings of the mosquitoes, for both the lean and blood-fed mosquitoes (Figure 2i,j; lean mosquito with ground: $F^*_{z,aero}$ = 0.69 ± 2.45; lean mosquito without ground: $F^*_{z,aero}$ = 0.69 ± 2.45; fed mosquito with ground: $F^*_{z,aero}$ = 0.69 ± 1.35; fed mosquito without ground: $F^*_{z,aero}$ = 0.69 ± 1.35). This suggests that throughout the take-off, the mosquito does affect the pressure distribution on the ground, but that the presence of the ground has no effect on the aerodynamic forces on the mosquito.

3.2 | Vertical forces

At the start of a take-off, mosquitoes are often pitched head down (Figure 3a,b) and during the take-off, they make a rapid pitch-up movement. As a consequence, the stroke-plane is oriented almost vertically at the start of the take-off and rotates towards a horizontal orientation near the end of the push-off phase. The path of the blood-fed mosquito has a relatively larger horizontal component compared to the lean mosquitoes (Figures 3a,b and 4a).

Comparing the computed aerodynamic force opposing the gravity vector $F^*_{z,aero}$ with the total vertical forces $F^*_{z,total}$ needed for the measured body accelerations (Figure 3c,e) shows that the large force fluctuation during the push-off originate from the ground forces on the legs and not from the aerodynamic forces acting on the wing. After push-off, the difference between the computed mean aerodynamic forces and the required aerodynamic forces (from inverse dynamics) are minimal and not significantly different from zero (one sample t test, p = 0.003), except for a short phase directly after lift-off in the case of the lean mosquito. This might originate from the filtering of the aerodynamic forces.

The average vertical force, aerodynamic force, and leg force during take-off (Figure 4c) show that both the legs and the wings make a contribution to force production throughout the push-off. The ratio between vertical aerodynamic forces and leg-induced push-off forces is not significantly different between lean and fed mosquitoes (Figure 4d; independent t test; p = 0.098). For both lean and blood-fed mosquitoes, the wings contribute 46% ± 11% (n = 13) to vertical force production throughout the push-off phase of a take-off.

The angle between the resultant force vector and the stroke-plane, known as the force angle ξ, was computed when the aerodynamic resultant force is larger than half of the body weight. In the case of the lean mosquito (Figure 3d), the force angle starts high at take-off and gradually decreases to around 90°. The blood-fed mosquito starts with a force vector more aligned to the body of the mosquito (Figure 3f). The average force

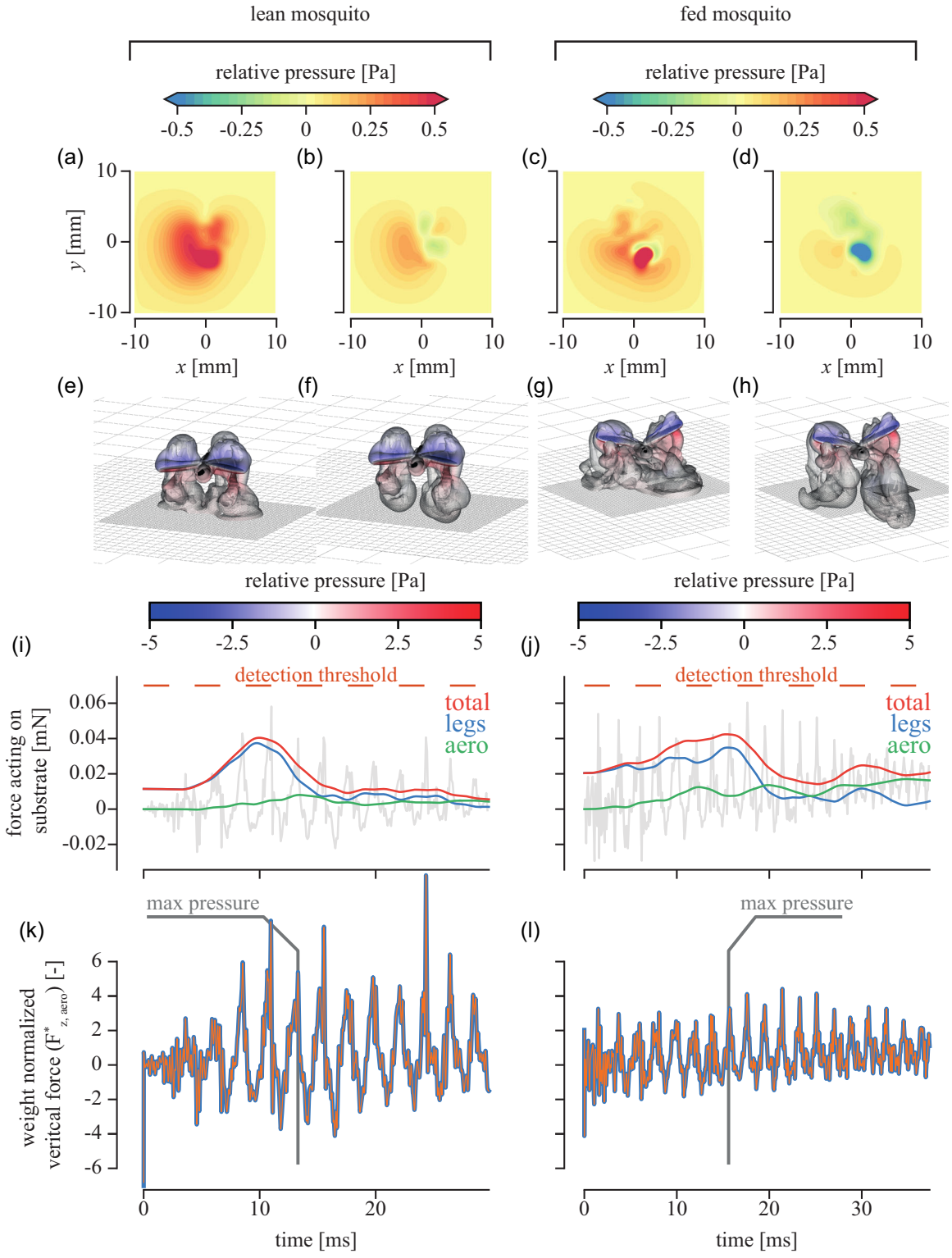

FIGURE 2 The effect of the ground on the aerodynamics of take-off maneuvers in malaria mosquitoes. (a–d) Maximum air pressure on the ground surface within a take-off maneuver of a lean mosquito, ((a, b) with and without ground, respectively) and a blood-fed mosquito ((c, d), with and without ground, respectively). See (k, l) for time at maximum pressure. (e–h) Equivalent wake structures at the point of maximum pressure on the ground, visualized using isosurfaces at the vorticity level of 1,000 s^{-1}, color-coded with local air pressure; (e) lean mosquito with ground, (f) lean mosquito without ground, (g) fed mosquito with ground, and (h) fed mosquito without ground. (i, j) Integrated pressure over a patch of 2 cm × 2 cm, for the lean and fed mosquito, respectively; light-gray lines are the aerodynamic forces, green lines are the wingbeat-average aerodynamic forces, blue lines are the forces exerted by the legs on the ground, and red lines the sum of the leg and wingbeat-average aerodynamic forces. (k, l) Normalized vertical aerodynamic forces of the lean and fed mosquito, respectively. Orange lines show results for simulations with the ground present, and blue lines are without ground [Color figure can be viewed at wileyonlinelibrary.com]

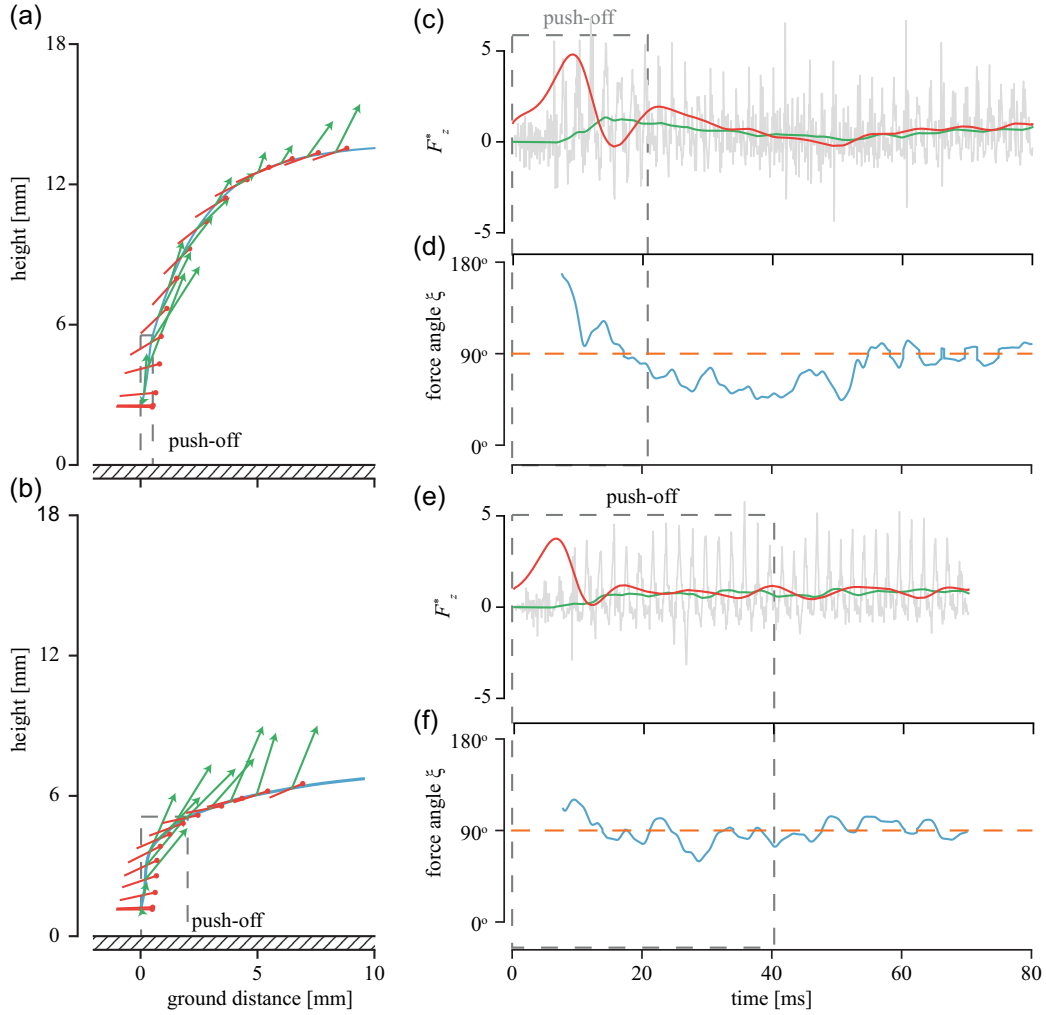

FIGURE 3 The kinematics and force dynamics throughout the take-off of an unfed and blood-fed malaria mosquito. (a, b) Take-off dynamics of a lean and blood-fed mosquito, respectively. The trajectories are shown by the blue curves, red lollipops indicate the body-axes at intervals of 5 ms, green arrows indicate the aerodynamic force vectors at each time interval, and the dashed gray box indicates the interval when at least one leg is still on the ground. (c, e) Normalized vertical forces for the lean and fed mosquito respectively, where total vertical forces based on the body acceleration are in red, aerodynamic forces throughout the wingbeats are in light-gray, and the wingbeat-average aerodynamic forces are in green. (d, f) Angle ξ between the mean aerodynamic force vector and the stroke-plane for the lean and fed mosquito, respectively; the horizontal dashed line indicates the 90° angle at which the force vector is perpendicular to the stroke-plane [Color figure can be viewed at wileyonlinelibrary.com]

angle during take-off for the fed mosquitoes is significantly lower than the lean mosquitoes (Figure 4b; fed mosquitoes: $\xi = 72.2° \pm 8.0°$, $n = 7$; lean mosquitoes: $\xi = 83.0° \pm 7.1°$, $n = 6$; independent t test, $p = 0.038$; Jones et al., 2001).

The resultant force, normalized with a standard mass of 1 mg, per wingbeat for both the lean and fed mosquitoes scales with the stroke amplitude (Figure 4f), and shows a significant positive correlation (simple linear regression, $p < 0.0001$). The deviation angle amplitude, the difference between the maximum and minimum deviation angle per wingbeat, also scales positively with the stroke amplitude (Figure 4g; simple linear regression, $p < 0.0001$). Finally, for all mosquitoes combined the force angle ξ scales negatively with the resultant force (Figure 4h, $p < 0.002$), although this correlation is absent in the two seperate groups.

3.3 | Pitch torques

During the take-off, all the measured mosquitoes are pitching up (Muijres et al., 2017). To initiate this pitch-up maneuver a mosquito needs to produce pitch-up torque and to stop this pitch-up rotation the animal should produce a pitch-down torque. To test how the mosquitoes produce these torques, we compared total pitch torques and the aerodynamic pitch torques throughout the take-off (Figure 5a,c). During the flight phase of the take-off, the wingbeat-average aerodynamic pitch torques do not significantly differ from the total torques ($\Delta T^*_{pitch} = -0.017 \pm 0.049$, $n = 12$, one sample t test, $p = 0.28$). This shows that our CFD method captures the aerodynamic torques well, allowing us to estimate pitch torques from leg push-off as the difference between total torque and aerodynamic torque. During

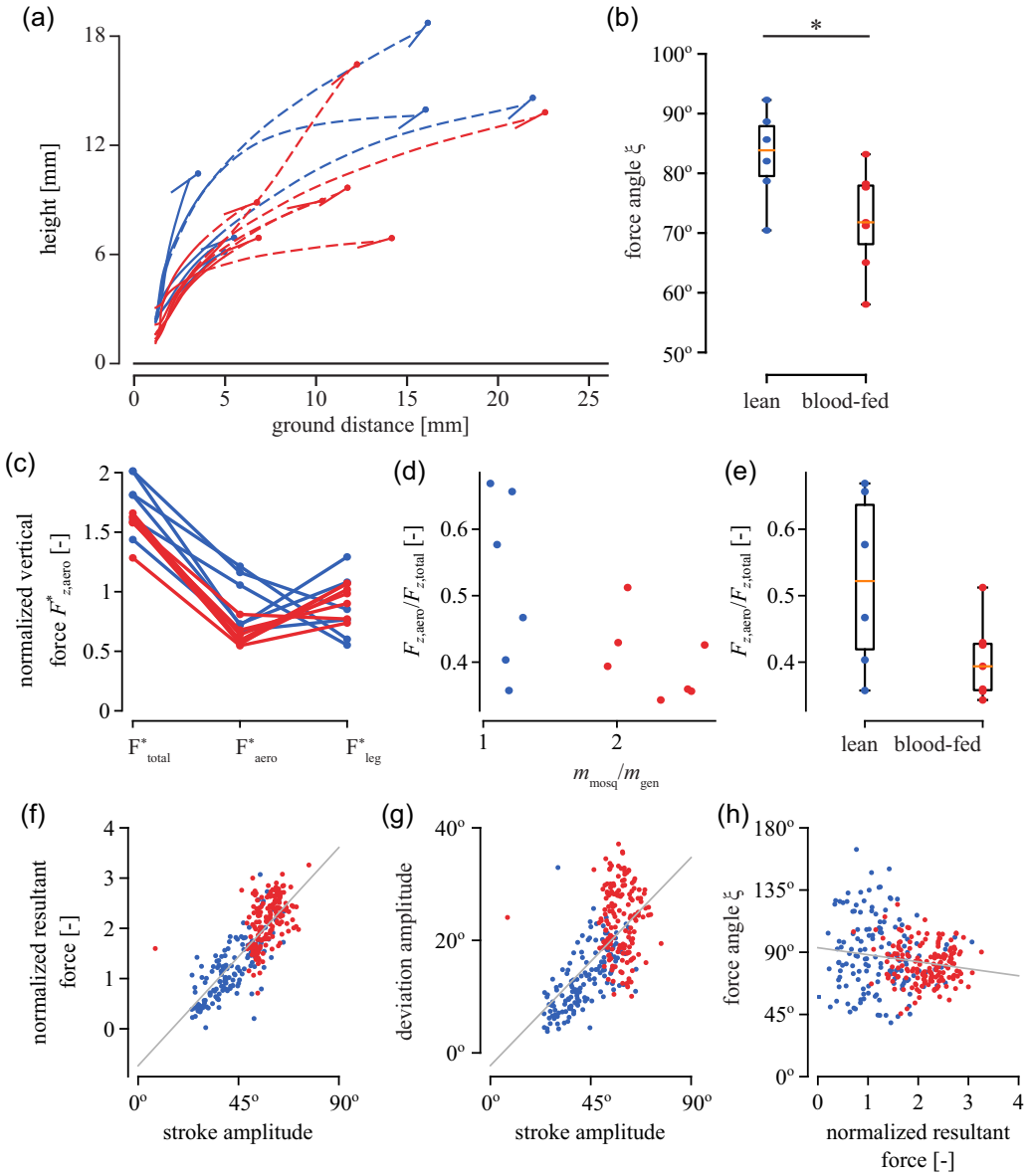

FIGURE 4 Kinematics and force dynamics throughout all simulated take-offs, where all data in blue refer to lean mosquitoes and red data refer to of fed mosquitoes. (a) Take-off trajectories, with solid line segments show the push-off phase and dashed line segment show the aerial phase; lollipops show body position and orientation at the end of the trajectory. (b) Average force angle ξ during the push-off. Asterisk indicates a significant difference (p=.038). (c) Mean normalized vertical force throughout the push-off phase of simulated take-offs, separated into total force, aerodynamic force, and leg-induced push-off force. (d) The ratio between the mean vertical aerodynamic force and mean vertical total force during the push-off phase against the normal body weight for all mosquitoes. (e) Average force ratio for the lean and the blood-fed mosquitoes. (f) Stroke amplitude against the normalized resultant aerodynamic forces. The gray line shows a simple linear regression fit with p<0.0001. (g) Stroke angle amplitude against the deviation angle amplitude. The gray line shows a simple linear regression fit with p<0.0001. (h) Force angle ξ against the normalized resultant aerodynamic force, the gray line is a simple linear regression with p=0.002 [Color figure can be viewed at wileyonlinelibrary.com]

the push-off phase, largest differences occur between total pitch torques and the aerodynamic pitch torques, suggesting that the leg push-off forces contribute to pitch torque production.

During the push-off phase, the total body pitch torque shows a positive pitch-up peak for both lean and blood-fed mosquitoes (Figure 5a,c). In the case of the lean mosquito, part of this torque is generated by the wings, but the aerodynamic torques are always lower than the total torques. The total torques produced by the blood-fed mosquito reveals a more dramatic dynamics, with a large pitch-up total torque followed by a pitch-down torque, which is not found in the corresponding aerodynamic torques (Figure 5c).

The pitch-up torque peaks at the start of the push-off phase are not different between the lean and blood-fed mosquitoes

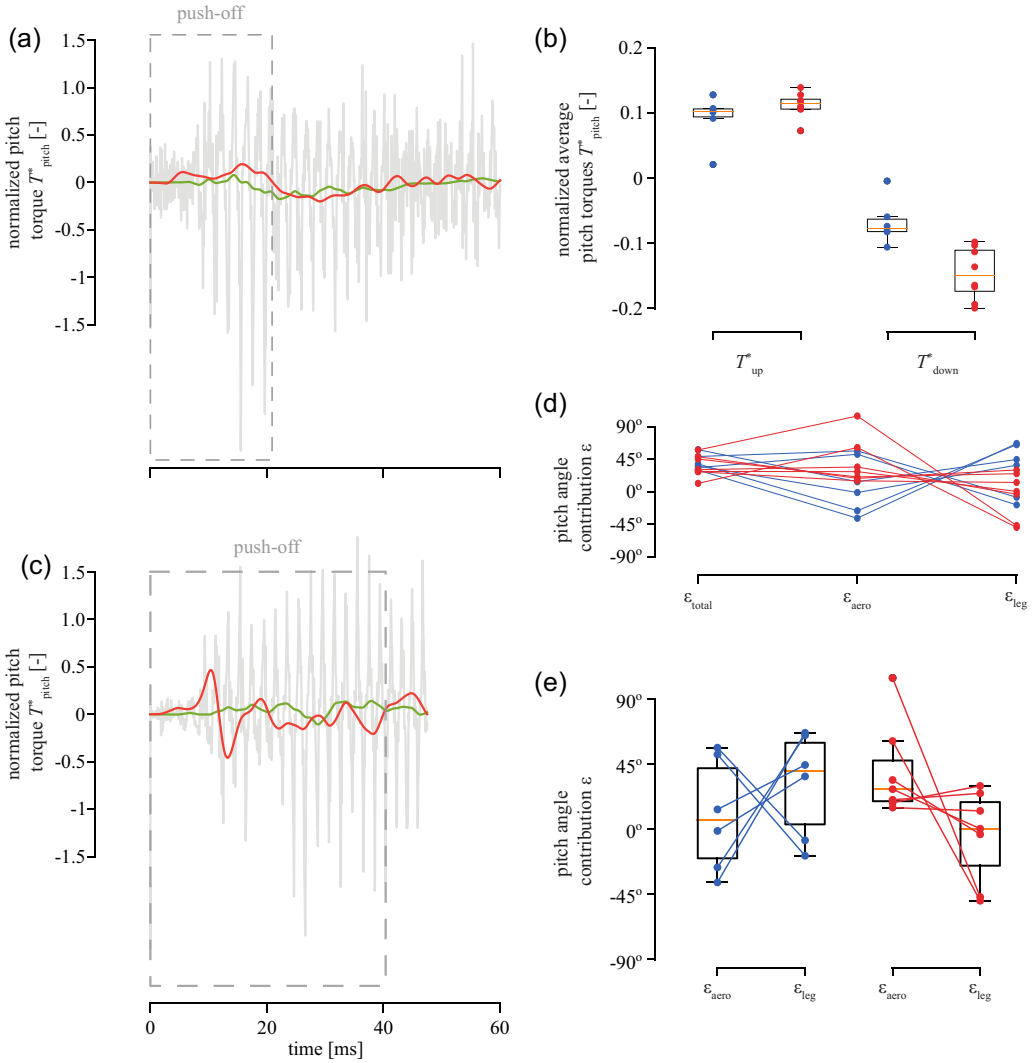

FIGURE 5 (a, c) Normalized pitch torques throughout the take-off of a lean and fed mosquito, respectively. Aerodynamic pitch torques throughout each wingbeat are in light-gray, the equivalent wingbeat-average aerodynamic torques are in green, and total pitch torques in red. The dashed box indicates the interval when at least one leg is still touching the ground. (b, d, e) Mean pitch torques produced during the push-off phase of all simulated take-offs; all data in blue are of lean mosquitoes and data in red are of fed mosquitoes. (b) Normalized average pitch-up torques and normalized average pitch-down torques during the push-off phase. (d) The contribution to the pitch-up movement throughout the push-off, of total pitch torque ε_{total}, aerodynamic pitch torque ε_{aero}, and leg-induced pitch torque ε_{leg}. (e) Pitch angle contribution for the wings (ε_{aero}) and legs (ε_{leg}), of lean mosquitoes (blue) and fed mosquitoes (red). All torques and angular momentum were normalized with the product of body weight and body length of the mosquito [Color figure can be viewed at wileyonlinelibrary.com]

($p = 0.208$, independent t test; Figure 5b), whereas the following pitch-down torque peaks are on average 2.16 times higher in the blood-fed mosquitoes, compared to the lean mosquitoes ($p = 0.002$, independent t test; Figure 5b).

On the basis of temporal dynamics of torque production, we determined the relative contribution of total pitch torque, leg-induced torque, and wing-induced torque to the pitch-up body reorientation (equation (6) and Figure 5d). The contribution of the total torques to the pitch angle (ε_{total}) is similar for both the lean and the fed mosquitoes (Figure 5d). The contribution of the aerodynamic torques to the pitch angle ε_{aero} is higher for the fed mosquitoes than for the lean mosquitoes, most likely due to a blood-load induced a backward shift of the center of mass relative to the aerodynamic center (Figure 5d). As a result, the blood-fed mosquitoes have a lower contribution of the legs to the pitch-up rotation ε_{leg} than the lean mosquitoes. In fact, on average, leg push-off in blood-fed mosquitoes even contribute negatively to the pitch-up maneuver (fed mosquitoes: $\varepsilon_{leg} = -4.7° \pm 29.7°$, $n = 7$), whereas for the lean mosquitoes the average leg-induced pitch-up contribution was positive (lean mosquitoes: $\varepsilon_{leg} = 31.0° \pm 33.1°$, $n = 6$).

Comparing the contribution of aerodynamic torques and leg push-off torques to the pitch-up movement within the push-off phase (Figure 5e) shows that the positive contribution of

aerodynamic torques, mostly present in the blood-fed mosquitoes, is compensated by a reduced (or even negative) pitch-up contribution from the legs.

4 | DISCUSSION

4.1 | Force production

During take-off, a mosquito has to produce high-enough forces to reach an escape velocity that maximizes the chance to escape a predator or a defensive blood host (Roitberg et al., 2003). These forces are generated by a combination of the aerodynamic forces produced by the flapping wings and ground push-off forces from the legs (Muijres et al., 2017; Smith et al., 2018). In our simulations, we compared the required forces needed to perform the measured take-off with the aerodynamic forces generated by the wings. Our results show that during the push-off phase of take-off, the vertical aerodynamic force indeed represents 46% ± 11% of the total take-off force ($n = 13$, Figure 4c). Interestingly, this fraction does not differ significantly between fed mosquitoes and lean mosquitoes ($p = 0.098$), which suggests that the aerodynamic and leg forces scale both with the body mass of the animal.

4.2 | Forces acting on the substrate

The take-off poses a large demand on the flight apparatus of particularly a blood-fed mosquito, because during take-off the animal has to generate a high-enough escape velocity while carrying a considerable payload. We explored whether the interaction of the wake with the substrate enhances the force generation of the wing, aiding in the take-off.

For this, we conducted two computational experiments; one for a lean and one for a fed mosquito. Both experiments consisted of two simulations; one with the ground present, and one without the ground present. Surprisingly the ground had no effect on the forces on the mosquito, even though the wake had a clear interaction with the substrate (Figure 2i–l). The change in the wake did not seem to propagate upstream to the flapping mosquito, which resulted in a similar airflow around the wings compared to the case without substrate present. This result is in line with a previous study on fruit flies (Kolomenskiy et al., 2016).

However, our result does show that the presence of the substrate increases the local pressure compared to an equivalent plane at the same location in free air. This means that the wake has an effect on the substrate, which is in line with previous hypotheses (Muijres et al., 2017). For the blood-fed mosquitoes, the force on the platform resulting from this air pressure increase is equal to the detection threshold for mammalian skin, which might suggest that blood-fed mosquitoes can be detected during take-off. However, this force does not act on a single point as it is distributed over a surface of 2 cm × 2 cm (Figure 2c). This spreading may cause that the peak force on the skin surface remains below the detection limit of a mammalian host, which is in line with the hypothesis that escaping hematophagous insects can use wing-induced aerodynamic forces to reduce the chance of being detected (Muijres et al., 2017).

4.3 | Adaptation of the wingbeat kinematics

Our second hypothesis was that the mosquito increases its shallow stroke amplitude to increase the aerodynamic force production. The stroke amplitude is strongly correlated with the wingbeat-average aerodynamic resultant forces (Figure 4f). Furthermore, the stroke amplitude is correlated positively with the deviation angle amplitude (Figure 4g), which implies that both the stroke angle and the deviation angle are adapted simultaneously. This combined adjustment of the stroke and deviation angle amplitude suggests that a relatively simple mechanism is used to increase the resultant forces. A similar mechanism to increase the aerodynamic forces was found in honeybees (Altshuler et al., 2005).

4.4 | Force angle alignment

Due to the higher weight of the abdomen during take-off, the pitch angle of a fed mosquito is in general higher than for unfed mosquitoes (Muijres et al., 2017). This higher pitch angle of the body leads to a higher angle between the stroke-plane and the ground, because the stroke-plane is fixed to the body axis of the animal (Figure 1e–g). The force angle (ξ) of blood-fed mosquitoes, the pitch angle between the force vector and the stroke-plane, is reduced significantly compared with lean mosquitoes (Figure 4b).

For the blood-fed mosquitoes, the decrease in force angle, aligning the force vector closer to the body axis, is correlated with the increase in aerodynamic force production (Figure 4h). At the same time, to increasing this aerodynamic force, blood-fed mosquitoes not only increase stroke amplitude (Figure 4f), but they also increase the deviation angle amplitude (Figure 4g). A recent study showed that such a change in deviation angle amplitude causes a pitch-down rotation of the force vector (Muijres et al., 2017). This suggests that blood-fed mosquitoes synchronize realignment of the force vector with an increase in force magnitude. This allows them to simultaneously compensate for both the weight increase and the higher body pitch angle as a result of flying with a blood load in their abdomen.

4.5 | Pitch control via leg push-off

During take-off, the mosquito has to pitch up rapidly to reorient its stroke-plane parallel to the ground, such that the force vector opposes the gravity vector (Muijres et al., 2017). This pitch-up motion occurs when the legs are still touching the ground. We

have found that both lean and fed mosquitoes use their legs for pitch-up control (Figure 5d). Interestingly, the lean mosquitoes achieve this pitch control via a positive contribution of leg torques to the pitch-up movement, whereas in fed mosquitoes the legs contribute on average negatively to the pitch-up movement (Figure 5e). This is most likely caused by a backward shift of the center of mass as a result of blood feeding (Figure 1c). Due to this, a blood-fed mosquito generates larger aerodynamic pitch-up torques, which need to be compensated by pitch-down torques produced by the legs at push-off (Figure 5b,c).

Fruit flies also generate a large pitch-up torque during take-off, where they rely solely on their legs. When the fruit fly is airborne it uses its wings to generate a counter torque to stop the pitch-up rotation of the body (Chen & Sun, 2014). On the contrary, mosquitoes produce pitch torques with both their legs and wings throughout the complete push-off phase. The pitch torque produced by the wings remains relatively constant throughout the take-off maneuver. For blood-fed mosquitoes, the leg-induced torques vary from positive when initiating the pitch-up maneuver, to negative when stopping the pitch-up rotation (Figure 5b,c).

This suggests that that malaria mosquitoes use their flight apparatus primarily as a motor system, whereas they use their legs to control the body pitch movements throughout take-off maneuvers. Together with the apparent coregulation of aerodynamic force magnitude and force angle, this suggests that malaria mosquitoes possess a robust control system that allows them to perform rapid take-off maneuvers both with and without a blood load in their abdomen.

ACKNOWLEDGMENT

We thank Cees Voesenek for his help and feedback during the analysis, Antoine Cribellier and Pulkit Goyal for the useful discussions, Sophia Chang and Jeroen Spitzen for the data measurements, Annelieke Wentzel and Steven ten Hoff for helping with the statistical analysis, and Henk Schipper for helping with organizing the computational resources. F. T. M. was supported by a grant from The Netherlands Organization for Scientific Research (NWO/VENI-863-14-007).

CONFLICT OF INTERESTS

The authors declare that there are no conflict of interests.

AUTHOR CONTRIBUTIONS

W. G. v. V. developed the computational system, carried out the simulations, analyzed the data, and drafted the manuscript. F. T. M. provided the mosquito data, coordinated the study and helped to draft the manuscript. All authors were involved in conceiving and designing the study, contributed critically to writing the manuscript and gave final approval for publication.

ORCID

Wouter G. van Veen http://orcid.org/0000-0002-9377-7040
Johan L. van Leeuwen http://orcid.org/0000-0002-4433-880X
Florian T. Muijres http://orcid.org/0000-0002-5668-0653

REFERENCES

Altshuler, D. L., Dickson, W. B., Vance, J. T., Roberts, S. P., & Dickinson, M. H. (2005). Short-amplitude high-frequency wing strokes determine the aerodynamics of honeybee flight. *Proceedings of the National Academy of Sciences of the United States of America*, *102*, 18213–18218.

Bhalla, A. P. S., Bale, R., Griffith, B. E., & Patankar, N. A. (2013). A unified mathematical framework and an adaptive numerical method for fluid-structure interaction with rigid, deforming, and elastic bodies. *Journal of Computational Physics*, *250*, 446–476.

Bomphrey, R. J., Nakata, T., Phillips, N., & Walker, S. M. (2017). Smart wing rotation and trailing-edge vortices enable high frequency mosquito flight. *Nature*, *544*, 92–95.

Card, G., & Dickinson, M. (2008). Performace trade-off in the flight initiation of *Drosophila*. *The Journal of Experimental Biology*, *211*, 341–53.

Chen, M.-W., & Sun, M. (2014). Wing/body kinematics measurement and force and moment analyses of the takeoff of fruitflies. *Acta Mechanica Sinica*, *30*(4), 495–506.

Clements, A. N. (2011). *The biology of mosquitoes*. London, UK: Chapman & Hall.

Dickinson, M. H., & Muijres, F. T. (2016). The aerodynamics and control of free flight manoeuvres in *Drosophila*. *Philosophical Transactions B*, *371*, 20150388.

Jones, E., Oliphant, T., & Peterson, P. D. (2001). SciPy: Open Source Scientific Tools for Python. http://www.scipy.org/

Karásek, M., Muijres, F. T., de Wagter, C., Remes, B. D. W., & de Croon, G. C. H. E. (2018). A tailless aerial robotic flapper reveals that flies use torque coupling in rapid banked turns. *Science*, *361*, 1089–1094.

Kolomenskiy, D., Maeda, M., Engels, T., Liu, H., Schneider, K., & Nave, J.-C. (2016). Aerodynamic ground effect in fruitfly sized insect takeoff. *PLOS One*, *11*, e0152072.

Li, L., Rutlin, M., Abraira, V. E., Cassidy, C., Kus, L., Gong, S., … Jankowski, M. P. (2011). The functional organization of cutaneous low-threshold mechanosensory neurons. *Cell*, *147*, 1615–27.

Mittal, R., & Iaccarino, G. (2005). Immersed boundary methods. *Annual Review Fluid Mechanics*, *37*, 239–261.

Muijres, F. T., Chang, S. W., van Veen, W. G., Spitzen, J., Biemans, B. T., Koehl, M. A. R., … Dudley, R. (2017). Escaping blood-fed malaria mosqtuitoes minimize tactile detection without compromising on take-off speed. *Journal of Experimental Biology*, *220*, 3751–3762.

Muijres, F. T., Elzinga, M. J., Melis, J. M., & Dickinson, M. H. (2014). Flies evade looming targets by executing rapid visually directed banked turns. *Science*, *344*, 172–177.

Pond, C. M. (1972). The initiation of flight in unrestrained locusts, *Schistocera gregaria*. *Journal of Comparative Physiology*, *80*(2), 163–178.

Roitberg, B. D., Mondor, E. B., & Tyerman, J. G. A. (2003). Pouncing spider, flying mosquito: Blood acquisition increases predation risk in mosquitoes. *Behavioral Ecology*, *14*, 736–740.

Smith, N. M., Clayton, G. V., Khan, H. A., & Dickerson, A. K. (2018). Mosquitoes modulate leg dynamics at takeoff to accomodate surface roughness. *Bioinspiration & Biomimetics*, *14*, 016007.

Sunada, S., Wtanabe, K. K., & Azuma, A. (1993). Performance of a butterfly in take-off flight. *Journal of Experimental Biology*, *183*, 249–277.

Takken, W. (1991). The role of olifaction in host-seeking of mosqtuioes: A review. *Insect Science Application*, *12*, 287–295.

van Veen, W. G., van Leeuwen, J. L., & Muijres, F. T. (2019). A chordwise offset of the wing-pitch axis enhances rotational aerodynamic forces on insect wings: A numerical study. *Journal of The Royal Society Interface*, *16*, 20190118.

SUPPORTING INFORMATION

Additional supporting information may be found online in the Supporting Information section.

How to cite this article: van Veen WG, van Leeuwen JL, Muijres FT. Malaria mosquitoes use leg push-off forces to control body pitch during take-off. *J. Exp. Zool.* 2020;333:38–49. https://doi.org/10.1002/jez.2308